PHYSICAL REVIEW C **73**, 031901(R) (2006)

Transverse momentum and rapidity dependence of Hanbury-Brown–Twiss correlations in Au+Au collisions at $\sqrt{s_{NN}} = 62.4$ and 200 GeV

B. B. Back,[1] M. D. Baker,[2] M. Ballintijn,[4] D. S. Barton,[2] R. R. Betts,[6] A. A. Bickley,[7] R. Bindel,[7] A. Budzanowski,[3] W. Busza,[4] A. Carroll,[2] Z. Chai,[2] M. P. Decowski,[4] E. García,[6] T. Gburek,[3] N. George,[1,2] K. Gulbrandsen,[4] S. Gushue,[2] C. Halliwell,[6] J. Hamblen,[8] M. Hauer,[2] G. A. Heintzelman,[2] C. Henderson,[4] D. J. Hofman,[6] R. S. Hollis,[6] R. Hołyński,[3] B. Holzman,[2] A. Iordanova,[6] E. Johnson,[8] J. L. Kane,[4] J. Katzy,[4,6] N. Khan,[8] W. Kucewicz,[6] P. Kulinich,[4] C. M. Kuo,[5] W. T. Lin,[5] S. Manly,[8] D. McLeod,[6] A. C. Mignerey,[7] R. Nouicer,[6] A. Olszewski,[3] R. Pak,[2] I. C. Park,[8] H. Pernegger,[4] C. Reed,[4] L. P. Remsberg,[2] M. Reuter,[6] C. Roland,[4] G. Roland,[4] L. Rosenberg,[4] J. Sagerer,[6] P. Sarin,[4] P. Sawicki,[3] H. Seals,[2] I. Sedykh,[2] W. Skulski,[8] C. E. Smith,[6] M. A. Stankiewicz,[2] P. Steinberg,[2] G. S. F. Stephans,[4] A. Sukhanov,[2] J.-L. Tang,[5] M. B. Tonjes,[7] A. Trzupek,[3] C. Vale,[4] G. J. van Nieuwenhuizen,[4] S. S. Vaurynovich,[4] R. Verdier,[4] G. I. Veres,[4] E. Wenger,[4] F. L. H. Wolfs,[8] B. Wosiek,[3] K. Woźniak,[3] A. H. Wuosmaa,[1] and B. Wysłouch[4]

(PHOBOS Collaboration)

[1]*Argonne National Laboratory, Argonne, Illinois 60439-4843, USA*

[2]*Brookhaven National Laboratory, Upton, New York 11973-5000, USA*

[3]*Institute of Nuclear Physics PAN, Kraków, Poland*

[4]*Massachusetts Institute of Technology, Cambridge, Massachusetts 02139-4307, USA*

[5]*National Central University, Chung-Li, Taiwan*

[6]*University of Illinois at Chicago, Chicago, Illinois 60607-7059, USA*

[7]*University of Maryland, College Park, Maryland 20742, USA*

[8]*University of Rochester, Rochester, New York 14627, USA*

(Received 1 September 2004; revised manuscript received 21 September 2005; published 27 March 2006)

Two-particle correlations of identical charged pion pairs from Au+Au collisions at $\sqrt{s_{NN}} = 62.4$ and 200 GeV were measured by the PHOBOS experiment at BNL Relativistic Heavy Ion Collider (RHIC). Data for the 15% most central events were analyzed with Bertsch-Pratt and Yano-Koonin-Podgoretskii parametrizations using pairs with rapidities of $0.4 < y_{\pi\pi} < 1.3$ and transverse momenta $0.1 < k_T < 1.4$ GeV/c. The Bertsch-Pratt radii R_o and R_ℓ decrease as a function of pair transverse momentum. R_o and R_s are independent of collision energy, while R_ℓ shows a slight increase. The source rapidity y_{YKP} scales roughly with the pair rapidity $y_{\pi\pi}$, indicating strong dynamical correlations.

DOI: 10.1103/PhysRevC.73.031901 PACS number(s): 25.75.Dw, 25.75.Gz

Recent experimental results from all four experiments at the BNL Relativistic Heavy Ion Collider (RHIC) have concluded that Au+Au collisions at the top RHIC energy ($\sqrt{s_{NN}} =$ 200 GeV) have produced an extremely hot and dense state of matter [1–4]. This matter may have degrees of freedom that are purely hadronic ("hadronic gas"), purely partonic [quark-gluon plasma (QGP)] or an admixture of both. Identical-particle correlation measurements [Hanbury-Brown–Twiss (HBT)] yield valuable information on the size, shape, duration, and spatiotemporal evolution of the emission source. Because the dynamics of a hadron gas and a QGP are naïvely expected to be quite different, HBT may allow us to discriminate between these three scenarios [5,6].

Experimentally, the correlation function $C(\mathbf{q})$ is defined as

$$C(\mathbf{q}) = \frac{\sigma d^6\sigma/d^3p_1 d^3p_2}{(d^3\sigma/d^3p_1)(d^3\sigma/d^3p_2)}, \qquad (1)$$

where $d^3\sigma/d^3p$ and $d^6\sigma/d^3p_1 d^3p_2$ are the single-particle and two-particle cross sections. The numerator is determined directly from data, while the denominator is constructed using a standard event-mixing technique.

$C(\mathbf{q})$ can be fit to the Bertsch-Pratt parametrization of a Gaussian source in three dimensions [6–8],

$$C(\mathbf{q}) = 1 + \lambda e^{-(q_o^2R_o^2 + q_s^2R_s^2 + q_\ell^2R_\ell^2 + 2q_oq_\ell R_{o\ell}^2)}, \qquad (2)$$

where q_ℓ is the component of $\mathbf{q}$ along the beam direction; q_o is the component along the pair transverse momentum $\vec{k}_T = \frac{1}{2}(\vec{p}_{T1} + \vec{p}_{T2})$; and q_s is the component orthogonal to the other two. The q_oq_ℓ cross-term vanishes only for symmetric collisions with acceptances centered around midrapidity. The λ parameter represents the correlation strength. According to the definitions of q_o and q_s, R_o probes a mixture of the spatial and temporal extent of the source, while R_s measures only the spatial component. In the special case of a boost-invariant, transparent, azimuthally symmetric source, the ratio R_o/R_s may be a good indicator of the duration of the emission of particles from the source. Quantitative predictions for this quantity from hydrodynamic and transport models have varied by over an order of magnitude [9,10], and mostly focused on values between 1.5–2.0, while the first results from RHIC at $\sqrt{s_{NN}} = 130$ GeV indicated a value near unity [11,12]. However, it should be noted that at least one early qualitative prediction for a small value of $R_o - R_s$ exists in the literature [13]. A more recent three-dimensional hydrodynamic calculation (including opacity and transverse flow) [14] also was unable to reproduce the experimentally measured values for R_o/R_s. The results at $\sqrt{s_{NN}} = 130$ GeV also were consistent with a monotonic increase of R_ℓ from AGS energies ($\sqrt{s_{NN}} \simeq$ 2–5 GeV), while R_o and R_s remained roughly constant. It is also possible to fit the experimental data

at RHIC to a variety of *ansätze* [15–17], but the interpretation remains an open question. The wealth of HBT data over a large number of variables and their experimentally-determined systematic dependencies continue to create new challenges for theorists and add yet more pieces to the "HBT puzzle".

The data reported here for Au+Au collisions at $\sqrt{s_{NN}} =$ 62.4 and 200 GeV were collected using the PHOBOS two-arm magnetic spectrometer during RHIC Run IV (2004) and Run II (2001), respectively. Details of the setup have been described previously [18]. The spectrometer arms are each equipped with 16 layers of silicon sensors, providing charged particle reconstruction both outside and inside a 2 T magnetic field. The two symmetric arms and frequent magnetic field polarity reversals allowed for a number of independent cross-checks in the two-particle correlation measurement. A two layer silicon detector covering $|\eta| < 0.9$ and 25% of the azimuthal angle provided additional information on the position of the primary collision vertex.

The primary event trigger was provided by two sets of 16 scintillator paddle counters, which covered a pseudorapidity range $3 < |\eta| < 4.5$. More information on PHOBOS event selection and centrality determination can be found in Refs. [19,20].

The details of the track reconstruction algorithm can be found in Refs. [21,22]. Events with a reconstructed primary vertex position between -12 cm $< z_{\rm vtx} < 10$ cm along the collision axis and -0.1 cm $< x_{\rm vtx} < 0.2$ cm and -0.05 cm $< y_{\rm vtx} < 0.2$ cm along the transverse directions (asymmetric due to the noncentered beam) were selected to optimize vertex-finding precision, track reconstruction efficiency, and momentum resolution. Only particles which traversed the entire spectrometer were used in the analysis. A 3σ cut on the distance of closest approach of each reconstructed track with respect to the primary vertex ($dca_{\rm vtx} < 0.35$ cm) was used to reject background particles from decays and secondary interactions. The final track selection was based on the χ^2 probability of a full track fit, taking into account multiple scattering and energy loss. The momentum resolution is $\Delta p/p \sim 1\%$ after all cuts.

Particle identification was based on the truncated mean of the specific ionization loss in the silicon detectors. To identify pions, a cut of $\pm 3\sigma$ away from the expected mean value of the specific ionization $\langle dE/dx \rangle$ for pions was applied. This is shown as the region between the solid black lines in Fig. 1. Possible contamination from other particle species was studied using HIJING 1.35 [23] and a GEANT 3.21 [24] simulation of the full detector, applying the same reconstruction procedures to Monte Carlo events and data. The simulations were corrected for differences in the particle abundances and p_T spectra between HIJING and measured data. For $p_T < 1$ GeV/c, which contributes more than 90% of the pairs even for the highest k_T bin, the integrated contamination from kaons is about 6% while protons contribute less than 0.5%. For $1.5 < p_T < 2.0$ GeV/c, the integrated contamination rises to about 30% and 25% for kaons and protons, respectively, but these particles contribute a negligibly small fraction of the pairs. Consequently, the only significant contributions to pairwise contamination are from Kπ pairs: 11%, 12%, and 24% for the low, middle, and high k_T bin, respectively. Contamination from (anti)proton-π pairs

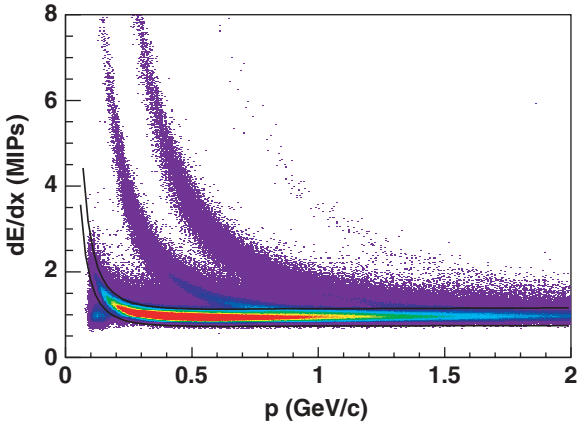

FIG. 1. (Color online) Distribution of the truncated average energy loss $\langle dE/dx \rangle$ as a function of reconstructed particle momentum. The region between the solid black lines corresponds to the $\pm 3\sigma$ cut used to select pions for this analysis.

is everywhere less than 4.5% and from like-sign pairs is less than 1.1%.

To reject ghost pairs, only one shared hit out of six in the inner spectrometer region (where track density is highest) and two shared hits out of five in the outer region were allowed per pair. A two-particle acceptance cut was applied to both data and background; the criterion for pair acceptance was defined by $|\Delta\phi| + 2|\Delta\theta| > 0.05$ rad, where $|\Delta\phi|$ and $|\Delta\theta|$ are the absolute values of the relative pair separation in azimuthal and polar angle, respectively. In this analysis, events in the most central 15% of the total inelastic cross-section were selected. HIJING was used to relate the fraction of the cross section to $\langle N_{\rm part} \rangle$, the mean number of participating nucleons [19]. The average number of participants for these events was estimated to be $\langle N_{\rm part} \rangle = 310$ (303) at $\sqrt{s_{NN}} = 200$ (62.4) GeV. About $7.3(3.3) \times 10^6\, \pi^+\pi^+$ and $5.5(3.0) \times 10^6\, \pi^-\pi^-$ pairs for $\sqrt{s_{NN}} = 200$ (62.4) GeV survive all cuts including centrality selection.

The event-mixed background is constructed by combining single tracks from randomly selected different events into fake pairs. Events from widely spaced collision vertices may yield a background that cannot reproduce the same phase space as the actual data. This effect is particularly prominent for a small-acceptance detector such as PHOBOS. In this analysis, an "event class" is defined solely by the vertex resolution of the detector. Events were defined as belonging to the same event class if they had vertices within 0.025 cm along the beam axis and 0.05 cm along the vertical and horizontal axes. Background events are only constructed from tracks mixed from the same event class.

Systematic errors (90% C.L.) were determined by changing cuts in two-particle acceptance and single-track azimuthal acceptance, using different random seeds for mixed-event background generation, as well as varying the event class definition to create background events from pairs with narrower and broader vertex ranges. Additionally, these studies were performed for each individual spectrometer arm and the differences included in the systematic uncertainties.

TABLE I. Bertsch-Pratt fit parameters for $\pi^+\pi^+$ and $\pi^-\pi^-$ in the rapidity range $0.4 < y_{\pi\pi} < 1.3$ for the 15% most central Au+Au collisions. Momenta are in GeV/c and radii are in fm. Errors are statistical (1σ) followed by systematic (90% C.L.).

Species	$\sqrt{s_{NN}}$	$\langle k_T \rangle$	λ	R_o	R_s	R_l	R_{ol}^2 (fm^2)
		0.198	$0.620 \pm 0.046 \pm 0.075$	$5.65 \pm 0.33 \pm 0.44$	$5.11 \pm 0.69 \pm 0.61$	$6.70 \pm 0.44 \pm 0.63$	$1.9 \pm 2.9 \pm 2.6$
$\pi^+\pi^+$	62.4 GeV	0.392	$0.660 \pm 0.055 \pm 0.069$	$4.72 \pm 0.34 \pm 0.48$	$4.74 \pm 0.45 \pm 0.42$	$4.53 \pm 0.31 \pm 0.31$	$0.85 \pm 1.7 \pm 2.2$
		0.680	$0.413 \pm 0.073 \pm 0.083$	$2.70 \pm 0.60 \pm 0.66$	$3.94 \pm 0.46 \pm 0.67$	$2.21 \pm 0.52 \pm 1.3$	$0.26 \pm 0.91 \pm 0.91$
		0.198	$0.574 \pm 0.042 \pm 0.057$	$5.79 \pm 0.33 \pm 0.33$	$4.85 \pm 0.73 \pm 0.57$	$6.17 \pm 0.40 \pm 0.76$	$2.2 \pm 2.9 \pm 2.9$
$\pi^-\pi^-$	62.4 GeV	0.391	$0.688 \pm 0.059 \pm 0.070$	$4.84 \pm 0.34 \pm 0.83$	$4.62 \pm 0.44 \pm 0.45$	$4.55 \pm 0.31 \pm 0.61$	$0.33 \pm 1.9 \pm 1.4$
		0.673	$0.532 \pm 0.075 \pm 0.13$	$3.58 \pm 0.51 \pm 1.1$	$4.21 \pm 0.48 \pm 0.53$	$2.53 \pm 0.32 \pm 0.36$	$-0.32 \pm 1.2 \pm 2.0$
		0.198	$0.493 \pm 0.028 \pm 0.041$	$5.48 \pm 0.27 \pm 0.36$	$4.09 \pm 0.63 \pm 0.66$	$6.75 \pm 0.33 \pm 0.26$	$4.9 \pm 2.3 \pm 5.7$
$\pi^+\pi^+$	200 GeV	0.393	$0.582 \pm 0.041 \pm 0.086$	$5.05 \pm 0.28 \pm 0.40$	$4.64 \pm 0.39 \pm 0.40$	$4.75 \pm 0.25 \pm 0.52$	$0.96 \pm 1.7 \pm 2.0$
		0.685	$0.444 \pm 0.049 \pm 0.082$	$3.31 \pm 0.32 \pm 0.52$	$3.96 \pm 0.36 \pm 0.20$	$2.98 \pm 0.29 \pm 0.37$	$0.25 \pm 1.1 \pm 1.5$
		0.198	$0.541 \pm 0.036 \pm 0.048$	$5.97 \pm 0.31 \pm 0.65$	$4.79 \pm 0.67 \pm 1.3$	$6.86 \pm 0.38 \pm 0.36$	$5.7 \pm 3.0 \pm 2.2$
$\pi^-\pi^-$	200 GeV	0.393	$0.559 \pm 0.044 \pm 0.054$	$4.59 \pm 0.30 \pm 0.43$	$4.26 \pm 0.39 \pm 0.31$	$4.89 \pm 0.32 \pm 0.49$	$1.1 \pm 1.9 \pm 3.0$
		0.690	$0.469 \pm 0.055 \pm 0.060$	$3.15 \pm 0.37 \pm 0.64$	$4.08 \pm 0.35 \pm 0.25$	$3.10 \pm 0.31 \pm 0.51$	$0.93 \pm 1.1 \pm 2.1$

Because the background is constructed from tracks belonging to different events, it does not *a priori* include multiparticle correlations (apart from a residual effect at the few percent level, which has been corrected following Refs. [25,26]). In order to study the HBT correlation, it is necessary to apply a weight to account for the Coulomb effect. The Coulomb correction can be expressed solely as a function of the invariant relative four-momentum $\mathbf{q}_{\rm inv}$,

$$F_{R_{\rm inv}}(\mathbf{q}_{\rm inv}) = \frac{F_c(\mathbf{q}_{\rm inv})}{F_{pl}(\mathbf{q}_{\rm inv})} = \frac{\int d\vec{r}\,|\psi_c(\vec{r})|^2 S(\vec{r})}{\int d\vec{r}\,|\psi_{pl}(\vec{r})|^2 S(\vec{r})}, \qquad (3)$$

where $S(\vec{r})$ is the distribution of the relative separation of the particle pairs at emission, $R_{\rm inv}$ is the radius parameter conjugate to $\mathbf{q}_{\rm inv}$, and ψ_c and ψ_{pl} are the Coulomb and plane wave-functions, respectively. A closed-form approximation and numerical interpolation for this relation was derived in Ref. [27] for $\lambda = 1$.

For variable λ [28],

$$F_{R_{\rm inv}}(\mathbf{q}_{\rm inv}, \lambda) = \frac{(1-\lambda) + \lambda\left(1 + e^{-\mathbf{q}_{\rm inv}^2 R_{\rm inv}^2}\right) F_{R_{\rm inv}}(\mathbf{q}_{\rm inv})}{1 + \lambda e^{-\mathbf{q}_{\rm inv}^2 R_{\rm inv}^2}}. \qquad (4)$$

This prescription was derived simultaneously and is nearly equivalent to the corrections applied by the CERES [29], STAR [30], and PHENIX experiments [31]; our results showed no significant change using either correction method. The method is applied iteratively, successively fitting distributions of the correlation function $C(\mathbf{q}_{\rm inv})$ and applying the fit values λ and $R_{\rm inv}$ to a new $S(\vec{r})$. Typically two or three iterations are sufficient for convergence.

The three-dimensional correlation functions were fit by Eq. (2) using MINUIT and the log-likelihood method. Table I shows the results of the fit for both $\pi^+\pi^+$ and $\pi^-\pi^-$. The data were analyzed in the longitudinal comoving system (LCMS) frame, defined as the frame in which the pair longitudinal momentum vanishes. In Fig. 2, the Bertsch-Pratt parameters and the ratio R_o/R_s are presented as a function of k_T for $\pi^-\pi^-$ pairs at $\sqrt{s_{NN}} = 62.4$ GeV and 200 GeV. The 200 GeV data are compared to data from STAR [30] and PHENIX [31]. Not shown are values for λ, which is roughly 0.5, and the cross-term R_{ol}^2, which is consistent with zero for all k_T bins. The small vertical acceptance of the PHOBOS detector roughly translates into a small acceptance in q_s, which is responsible for the large statistical and systematic uncertainties on the value of R_s at low k_T. The values of R_o and R_ℓ decrease rapidly with increasing

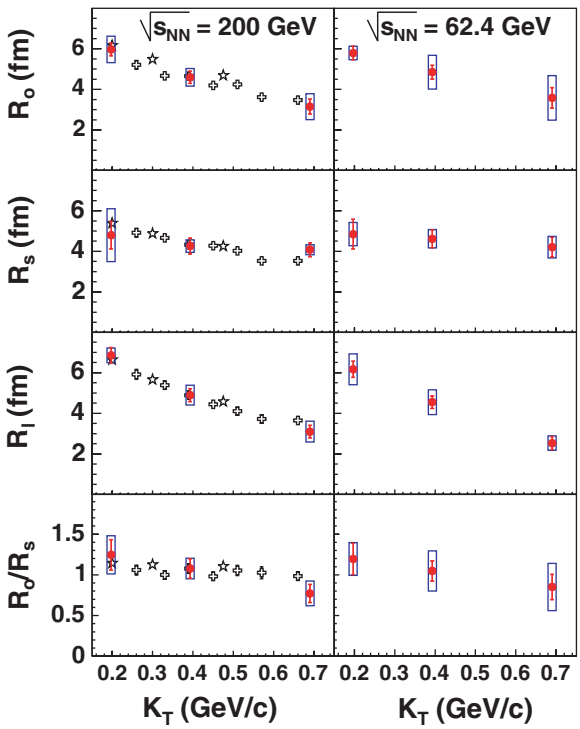

FIG. 2. (Color online) Bertsch-Pratt parameters R_o, R_s, R_ℓ and the ratio R_o/R_s for $\pi^-\pi^-$ pairs at $\sqrt{s_{NN}} = 200$ GeV (left panel) and 62.4 GeV (right panel) as a function of $\langle k_T \rangle$. For comparison, data from STAR [30] (open stars) and PHENIX [31] (open crosses) are presented at 200 GeV. PHOBOS systematic errors (90% C.L.) are shown as boxes; systematic errors from STAR and PHENIX are not shown.

k_T. The values of R_s and the ratio R_o/R_s are consistent with the results from STAR and PHENIX. It should be noted that the STAR and PHENIX data are measured at midrapidity while the PHOBOS data are measured at $\langle y_{\pi\pi}\rangle = 0.9$; additionally, STAR, PHOBOS, and PHENIX data are from the top 10%, 15%, and 30% of the cross section, respectively.

Despite the very different experimental acceptances, the data at 200 GeV agree remarkably well. The trends at $\sqrt{s_{NN}} = 62.4$ GeV are qualitatively and quantitatively similar to those at 200 GeV, except that R_ℓ may be slightly smaller.

The Bertsch-Pratt parameters λ, R_o, R_s, and R_ℓ are presented in Fig. 3 as a function of center of mass energy from $\sqrt{s_{NN}} = 2$ to 200 GeV [11,12,27,29–35]. The data are $\pi^-\pi^-$ pairs near midrapidity for comparable k_T bins from nine different experiments. The data at $\sqrt{s_{NN}} = 62.4$ GeV begin to fill the large gap between the top SPS energy and the 130 GeV RHIC data. The large systematic deviations between experiments preclude any strong statement on any sharp discontinuities as a function of $\sqrt{s_{NN}}$.

The correlation function was also fit to the Yano-Koonin-Podgoretskii (YKP) parametrization [36,37]

$$C(\mathbf{q}) = 1 + \lambda e^{-(q_\perp^2 R_\perp^2 + \gamma^2(q_\parallel - \beta q_\tau)^2 R_\parallel^2 + \gamma^2(q_\tau - \beta q_\parallel)^2 R_\tau^2)}, \qquad (5)$$

where β is the longitudinal velocity of the source and $\gamma = 1/\sqrt{1-\beta^2}$, $q_\perp$ and $q_\parallel$ are the relative three-momentum difference projected in the transverse and longitudinal directions, respectively, and q_τ is the relative difference in energy. Employing this coordinate system provides the advantange of factorizing the velocity and duration of the source from the spatial parameters. In addition to fits in the LCMS frame, data were also fit in the laboratory frame as a cross-check and yielded consistent results.

Table II shows the results of Yano-Koonin-Podgoretskii fits for $\pi^+\pi^+$ and $\pi^-\pi^-$ at both energies. In Fig. 4, the value of the source rapidity y_{YKP} [as extracted from β in Eq. (5)] is plotted as a function of pair rapidity for $\pi^-\pi^-$ pairs with $0.1 < k_T < 1.4$ GeV/c. The data from NA49 [38] at $\sqrt{s_{NN}} = 17.2$ GeV are also plotted; however, it should be noted the NA49 data presented here cover only $0.1 < k_T < 0.2$ GeV/c. The source rapidity scales with the rapidity of the pair, indicating the presence of strong position-momentum correlations. A static source would exhibit no correlation and would correspond to a horizontal line ($y_{\mathrm{YKP}} = 0$). A source with strong dynamical correlations would correspond to a straight line along $y_{\mathrm{YKP}} = y_{\pi\pi}$. The data are consistent with the latter scenario: Particles emitted at a given rapidity were produced by a source moving collectively at the same rapidity. In conclusion, we have measured HBT parameters in

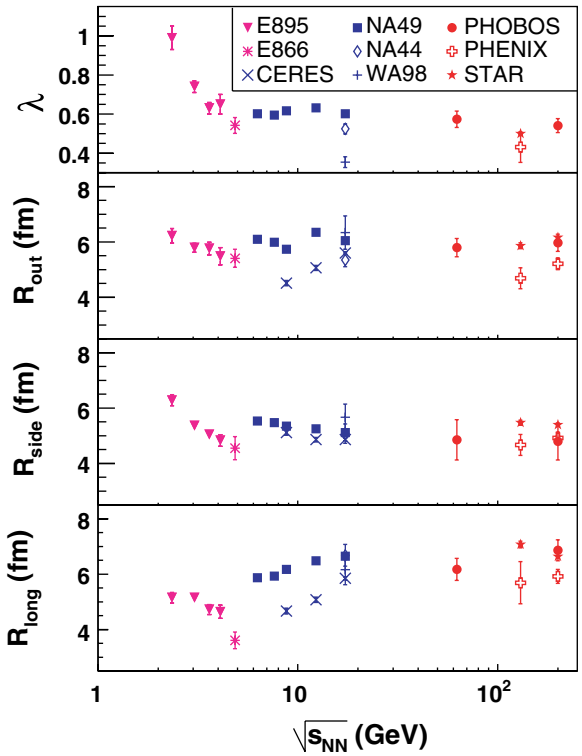

FIG. 3. (Color online) Bertsch-Pratt parameters λ, R_s, R_o, and R_ℓ as a function of $\sqrt{s_{NN}}$ for $\pi^-\pi^-$ pairs. The presented data are near midrapidity and represent comparable k_T bins from each experiment [11,12,27,29–35]. PHOBOS data are represented by solid circles. Systematic errors are not shown.

TABLE II. Yano-Koonin-Podgoretskii fit parameters for $\pi^+\pi^+$ and $\pi^-\pi^-$ in the k_T range $0.1 < k_T < 1.4$ GeV/c for the 15% most central Au+Au collisions. Radii are in fm. Errors are statistical (1σ) followed by systematic (90% C.L.).

Species	$\sqrt{s_{NN}}$	$\langle y_{\pi\pi}\rangle$	λ	$R_\perp$	$R_\parallel$	R_τ	β
		0.602	$0.669 \pm 0.057 \pm 0.074$	$5.05 \pm 0.33 \pm 0.30$	$5.75 \pm 0.45 \pm 0.70$	$0.0017 \pm 2.0 \pm 1.4$	$-0.162 \pm 0.086 \pm 0.11$
$\pi^+\pi^+$	62.4 GeV	0.879	$0.512 \pm 0.051 \pm 0.10$	$4.21 \pm 0.62 \pm 0.52$	$4.88 \pm 0.44 \pm 0.48$	$3.7 \pm 1.3 \pm 3.0$	$0.119 \pm 0.095 \pm 0.091$
		1.124	$0.506 \pm 0.046 \pm 0.062$	$3.96 \pm 0.42 \pm 0.41$	$5.20 \pm 0.47 \pm 0.58$	$3.0 \pm 1.0 \pm 2.0$	$-0.0738 \pm 0.080 \pm 0.082$
		0.602	$0.596 \pm 0.055 \pm 0.067$	$4.40 \pm 0.70 \pm 1.0$	$5.07 \pm 0.44 \pm 0.41$	$4.3 \pm 1.2 \pm 1.3$	$-0.0266 \pm 0.079 \pm 0.098$
$\pi^-\pi^-$	62.4 GeV	0.878	$0.539 \pm 0.054 \pm 0.080$	$4.78 \pm 0.64 \pm 0.69$	$5.10 \pm 0.48 \pm 0.82$	$0.75 \pm 6.4 \pm 2.6$	$0.0105 \pm 0.13 \pm 0.23$
		1.124	$0.525 \pm 0.044 \pm 0.040$	$4.09 \pm 0.44 \pm 0.47$	$4.84 \pm 0.35 \pm 0.25$	$3.3 \pm 0.99 \pm 2.0$	$-0.0687 \pm 0.075 \pm 0.048$
		0.602	$0.507 \pm 0.037 \pm 0.056$	$4.83 \pm 0.53 \pm 0.48$	$5.54 \pm 0.37 \pm 0.36$	$2.3 \pm 1.7 \pm 2.3$	$-0.0967 \pm 0.077 \pm 0.087$
$\pi^+\pi^+$	200 GeV	0.878	$0.441 \pm 0.034 \pm 0.088$	$4.36 \pm 0.53 \pm 0.73$	$5.37 \pm 0.37 \pm 0.82$	$1.3 \pm 2.9 \pm 2.2$	$-0.130 \pm 0.091 \pm 0.23$
		1.119	$0.454 \pm 0.031 \pm 0.032$	$3.89 \pm 0.37 \pm 0.59$	$5.03 \pm 0.31 \pm 0.43$	$3.6 \pm 0.70 \pm 1.0$	$-0.115 \pm 0.058 \pm 0.069$
		0.602	$0.492 \pm 0.040 \pm 0.042$	$3.83 \pm 0.55 \pm 0.44$	$5.43 \pm 0.38 \pm 0.45$	$4.4 \pm 0.96 \pm 1.3$	$0.0270 \pm 0.070 \pm 0.056$
$\pi^-\pi^-$	200 GeV	0.877	$0.485 \pm 0.042 \pm 0.079$	$4.50 \pm 0.50 \pm 0.70$	$5.23 \pm 0.40 \pm 0.71$	$2.3 \pm 1.6 \pm 1.7$	$-0.146 \pm 0.090 \pm 0.14$
		1.122	$0.469 \pm 0.040 \pm 0.044$	$4.16 \pm 0.44 \pm 0.31$	$5.72 \pm 0.43 \pm 0.57$	$2.2 \pm 1.3 \pm 0.90$	$-0.193 \pm 0.080 \pm 0.11$

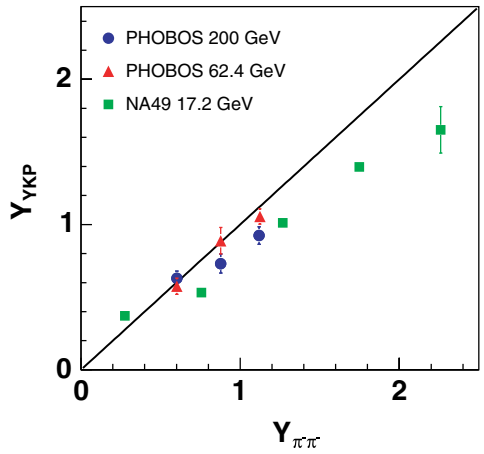

FIG. 4. (Color online) Dependence of the source rapidity y_{YKP} vs the pair rapidity $y_{\pi\pi}$ for PHOBOS at 200 GeV (circles), PHOBOS at 62.4 GeV (triangles), and NA49 (negatively charged hadrons) at 17.2 GeV [38] (squares).

Au+Au collisions with the PHOBOS detector using both the Bertsch-Pratt and Yano-Koonin-Podgoretskii parametrizations at energies of $\sqrt{s_{NN}} = 62.4$ and 200 GeV. The ratio R_o/R_s does not show significant deviation from unity over the entire k_T range. The data at 200 GeV show a nice agreement between three RHIC experiments with different acceptances, centrality measures, and rapidity, which implies that the source parameters are fairly insensitive to these variables at this energy. Additionally, the Bertsch-Pratt parameters evolve smoothly as a function of $\sqrt{s_{NN}}$ over nearly two orders of magnitude.

This work was partially supported by U.S. DOE grants DE-AC02-98CH10886, DE-FG02-93ER40802, DE-FC02-94ER40818, DE-FG02-94ER40865, DE-FG02-99ER41099, and W-31-109-ENG-38, by U.S. NSF grants 9603486, 0072204, and 0245011, by Polish KBN grant 1-P03B-062-27(2004-2007), and by NSC of Taiwan Contract NSC 89-2112-M-008-024.

[1] B. B. Back *et al.*, Phys. Rev. Lett. **91**, 072302 (2003).
[2] S. S. Adler *et al.*, Phys. Rev. Lett. **91**, 072303 (2003).
[3] J. Adams *et al.*, Phys. Rev. Lett. **91**, 072304 (2003).
[4] I. Arsene *et al.*, Phys. Rev. Lett. **91**, 072305 (2003).
[5] S. Pratt, Phys. Rev. Lett. **53**, 1219 (1984).
[6] S. Pratt, Phys. Rev. D **33**, 1314 (1986).
[7] G. Bertsch, Nucl. Phys. **A498**, 173 (1989).
[8] S. Chapman, P. Scotto, and U. Heinz, Phys. Rev. Lett. **74**, 4400 (1995).
[9] D. H. Rischke and M. Gyulassy, Nucl. Phys. **A608**, 479 (1996).
[10] S. Soff, S. A. Bass, and A. Dumitru, Phys. Rev. Lett. **86**, 3981 (2001).
[11] C. Adler *et al.*, Phys. Rev. Lett. **87**, 082301 (2001).
[12] K. Adcox *et al.*, Phys. Rev. Lett. **88**, 192302 (2002).
[13] T. Csörgő and L. P. Csernai, Phys. Lett. **B333**, 494 (1994).
[14] K. Morita and S. Muroya, Prog. Theor. Phys. **111**, 93 (2004).
[15] M. Csanád *et al.*, J. Phys. G **30**, S1079 (2004).
[16] F. Retière and M. A. Lisa, Phys. Rev. C **70**, 044907 (2004).
[17] T. Renk, Phys. Rev. C **69**, 044902 (2004).
[18] B. B. Back *et al.*, Nucl. Instrum. Methods A **499**, 603 (2003).
[19] B. B. Back *et al.*, Phys. Rev. Lett. **85**, 3100 (2000).
[20] B. B. Back *et al.*, Nucl. Phys. **A698**, 555 (2002).
[21] B. B. Back *et al.*, Phys. Rev. Lett. **87**, 102301 (2001).
[22] B. B. Back *et al.*, Phys. Lett. **B578**, 297 (2004).
[23] M. Gyulassy and X. N. Wang, Comput. Phys. Commun. **83**, 307 (1994).
[24] GEANT 3.2.1, CERN program library.
[25] W. Zajc *et al.*, Phys. Rev. C **29**, 2173 (1984).
[26] V. Cianciolo, Ph.D. thesis, M.I.T. (1994).
[27] L. Ahle *et al.*, Phys. Rev. C **66**, 054906 (2002).
[28] B. Holzman *et al.*, J. Phys. G **30**, S1049 (2004).
[29] D. Adamová *et al.*, Nucl. Phys. **A714**, 124 (2003).
[30] J. Adams *et al.*, Phys. Rev. Lett. **93**, 012301 (2004).
[31] S. S. Adler *et al.*, Phys. Rev. Lett. **93**, 152302 (2004); nucl-ex/0401003.
[32] M. A. Lisa *et al.*, Phys. Rev. Lett. **84**, 2798 (2000).
[33] I. G. Bearden *et al.*, Phys. Rev. C **58**, 1656 (1998).
[34] S. Kniege *et al.*, J. Phys. G **30**, S1073 (2004); nucl-ex/0403034.
[35] M. M. Aggarwal *et al.*, Eur. Phys. J. C **16**, 445 (2000).
[36] F. Yano and S. Koonin, Phys. Lett. **B78**, 556 (1978).
[37] M. Podgoretskii, Sov. J. Nucl. Phys. **37**, 272 (1983).
[38] H. Appelshäuser *et al.*, Eur. Phys. J. C **2**, 661 (1998).